Turkish Journal of Chemistry

http://journals.tubitak.gov.tr/chem/

Research Article

Turk J Chem
(2015) 39: 395 – 411

doi:10.3906/kim-1405-65

Gaseous and dissolved oxygen sensing with stabilized pyrene in ionic liquid modified electrospun slides

Özlem ÖTER[1,*], **Gülhan SABANCI ŞAHİN**[2]

[1]Department of Chemistry, Faculty of Science, Dokuz Eylül University, Kaynaklar Campus, Buca, İzmir, Turkey
[2]The Graduate School of Natural and Applied Sciences, Dokuz Eylül University, Kaynaklar Campus, Buca, İzmir, Turkey

Received: 23.05.2014 • **Accepted/Published Online:** 15.01.2015 • **Printed:** 30.04.2015

Abstract: Pyrene dye has many superior characteristics for oxygen sensing studies such as long fluorescence lifetime, high quantum yield, and good sensitivity. It is preferred in some cases over ruthenium dyes for its more lipophilic character and higher sensitivity. However, easy photodegradation of pyrene is a challenging problem. In this study, pyrene dye was for the first time immobilized in an ethyl cellulose matrix and used for oxygen sensing in the form of thin films and electrospun sensing slides. The hydrophobic ionic liquid 1-butyl-3-methylimidazolium hexafluorophosphate was used as additive for the first time for dissolved oxygen sensing studies. The oxygen sensitivity of the dye was evaluated with both steady state- and fluorescence lifetime-based measurements. The sensing slides were stable for 45 min under continuous irradiation and could be stored for 100 days under ambient laboratory conditions. This storage time is the longest reported lifetime for pyrene-based sensors. The enhanced stability can be attributed to the presence of ionic liquid, which behaves like a sink for oxidative, reductive, acidic, and/or basic effects. The sensor response time was between 6 and 20 s, depending on the oxygen concentration. The method can be applied for both dissolved and gaseous oxygen measurements.

Key words: Optical oxygen sensor, fluorescence, fluorescence lifetime, ionic liquid, electrospinning, pyrene dye

1. Introduction

Remote sensing and continuous monitoring of accurate amounts of gaseous and dissolved oxygen is of great significance in industrial, environmental, and biomedical processes.[1] Optical chemical sensors are very advantageous and widely used for sensing of oxygen because of their short response times, ease of fabrication, efficient sensitivity, and low costs. Many of these sensors are based on the oxygen quenching of fluorescence of different organic dyes.

Recently, oxygen sensing has also been utilized for measuring surface pressure distribution in wind tunnel models.[2,3] The basic principle of pressure sensitive paint is the oxygen quenching of fluorescence. Pyrene dye and its derivatives are extensively used for oxygen sensing purposes because of their long fluorescence lifetimes, high fluorescence quantum yields, and high oxygen sensitivities.[4–13] Some of these studies are solution phase studies, which do not supply a stable environment for sensor applications because of evaporation of the solvent etc.[12,13] Moreover, pyrene-based dyes usually suffer from instability due to loss of dye not only from the aqueous matrix but also from the solid matrix by evaporation or sublimation. Clark et al. have intensively studied the

*Correspondence: ozlem.oter@deu.edu.tr

solution medium effects on the photochemical degradation of pyrene in water.[14] Kubat et al. investigated the degradation of pyrene by UV radiation.[15]

Hence, some studies were conducted in order to prepare new and stable derivatives of pyrene and/or in order to increase the stability of pyrene by testing different additives or matrix materials. Table 1 contains comparative data regarding the type of sensitive dye, matrix material, sensitivity, dynamic working range, and stability from some recently published literature. Basu et al. synthesized a new pyrene derivative, 1-decyl-4-(1-pyrenyl) butanoate (DPB), and investigated its photophysical properties in toluene and in silicone polymers. They suggested the new dye as a potential substitute for pyrene in pressure-sensitive paints.[2] Fujiwara and Amao fabricated some pyrene derivatives as luminescence probes for oxygen sensing and investigated their oxygen sensing properties.[4,5,7,16] They worked with water soluble derivatives of the pyrene dye; thus their proposed sensor was for only gaseous oxygen sensing. They obtained high sensitivity values; however, the Stern–Volmer plots were not linear in the concentration range of 0.0%–100.0% O_2 (g).[4] Furthermore, they did not report any long-term storage time or any time-resolved fluorescence data for their sensor. Bekiari and Lianos proposed a glass slide dip-coated in a solution of reversed micelles in cyclohexane containing titanium(IV) tetraisopropoxide. However, they did not report the oxygen sensing and stability characteristics of the slide.[17] Basu and Rajam compared the oxygen sensor performance of some pyrene derivatives in a silicone polymer matrix. They reported the emission-based characteristics of the silicone coatings of pyrene derivatives but they did not investigate the oxygen sensing capability of the silicone-doped pyrene derivatives.[18] Hrdlovi et al. also have reported the spectral properties of a novel fluorescence probe based on pyrene both in solution and in polymer matrices.[19]

In the scope of the recent literature, there is a lack of studies that investigate the stability and O_2 sensing characteristics of pyrene dye in solid matrices. It is well known that the sensing properties of sensors strongly depend on the type and properties of polymer matrices and on their probable modifications. Recently, the fabrication of mesoporous, micro- and nanosized materials for gas sensing is an increasing trend.[20–25] Moreover, as green chemistry reagents, ionic liquids have superior characteristics for the modification of these matrices.[26–32] In our previous studies, we compared the performance of electrospun fibers with conventional thin films as solid matrix materials for optical chemical sensor designs. We observed that the utilization of nano- and microporous structures enhanced the stability and sensitivity of the sensor.[33,34] In the present study, we fabricated the nanoporous film structures and the microscale porous materials of polymers by electrospinning method for the sensitive detection of gaseous and dissolved oxygen with pyrene dye in a large concentration range. The sensitivity of the dye was evaluated both with steady state and fluorescence lifetime based measurements. This is the first study of oxygen sensing with pyrene in electrospun sensing slides. Additionally, we employed the hydrophobic ionic liquid 1-butyl-3-methylimidazolium hexafluorophosphate for the first time as additive of sensor matrix for dissolved oxygen measurements. The ionic liquid enhanced the sensitivity, stability, and robustness of unstable pyrene dye for both dissolved and gaseous oxygen analysis. The storage lifetime of pyrene extended to 100 days when stored under ambient laboratory conditions. This time is the longest reported lifetime for pyrene-based sensors. The hydrophilic ionic liquids were also tested and evaluated for gaseous oxygen sensing purposes.

Table 1. Comparison of the O_2 sensing properties of different sensors.

Sensitive dye	Matrix material	Sensitivity	Dynamic working range	Stability	Ref.
pyrene-1 decanoic acid		$I_0/I = 50.7$ $K_{sv1} = 1.5\%^{-1}$ $K_{sv2} = 0.0030\%^{-1}$			
pyrene-1 dodecanoic acid	chemisorption layers onto aluminum plate	$I_0/I = 44.7$ $K_{sv1} = 2.30\%^{-1}$ $K_{sv2} = 0.0011\%^{-1}$	100.0% argon to 100.0% oxygen [%]	With continuous irradiation: 24 h	4
pyrene-1 butyric acid		$I_0/I = 73.4$ $K_{sv1} = 2.00\%^{-1}$ $K_{sv2} = 0.0016\%^{-1}$			
1-pyrene butylic acid/ mystric acid	Nanoporous anodic oxidized aluminum plate	$I_0/I_{100} = 73.4$ at 461 nm; [MA]/[PBA] = 0	100.0% N_2 to 100.0% O_2 [%]	Not mentioned	5
pyrene-1 decanoic acid	pyrene-1 decanoic acid onto aluminum plate	$I_0/I = 36.6$	100.0% argon to 100.0% oxygen [%]	With continuous irradiation: 24 h	7
pyrene carboxylic acid with long alkyl chain (1-pyrenedecanoic acid and 1-pyrenedodecanoic acid)/myristic acid	the anodic oxidation of aluminum plate	$K_{SV} = 1.2 \times 10^{-1}(\%^{-1})$	Parabolic for 100.0% N_2 to 100.0% O_2 [%]		16
1-pyrenyl methanol 1-pyrenyl butanol 1-pyrene butyric acid 1-pyrene acetic acid	silicone polymer matrix	$I_0/I = 1.82$ (at 479 nm) $I_0/I = 3.32$ (at 479 nm) $I_0/I = 1.1$ (at 476 nm) $I_0/I = 1.09$ (at 476 nm)	100% N_2 and 21% O_2 [%].	Not mentioned	19
pyrene-1-butyric acid	pyrene-1-butyric acid - doped polyaniline	$K_{SV} = 1.32 \pm 0.09$	0–7 mbar O_2	Not mentioned	20
[Ru(Phen)2Phen-Si]2+ (Phen = 1,10-phenanthroline, Phen-Si = 2-[4-{3-(triethoxysilyl)propyl} phenyl] imidazo [4,5-f]-1,10-phenanthroline)	Functionalized mesoporous MSU-3 backbones in presence of Pluronic P123 surfactant	$I_0/I_{100} = 9.8$	100.0% N_2 to 100.0% O_2 [%]	Xe lamp irradiation ≈ 3600 s at 25 °C	21
Ru(Bphen)2bpy]2+ (Bphen = 4,7-diphenyl-1,10-phenanthroline, bpy = 2,20-bipyridyl)	Ordered functionalized mesoporous material, MCM-41		100% N_2 to 100.0% O_2 [%]	Stability in solvent: 5 days	22
Ruthenium(II)-tris (4,7-diphenyl-1,10-phenanthroline)] dichloride, phase fluorescence	Fluorinated and nonfluorinated sol gel films	For nonfluorinated films; $K_{SV} = 0.094 \pm 0.001$ for fluorinated films; $K_{SV} = 0.208 \pm 0.003$ $(O_2\%^{-1})$	100.0% N_2 to 5.0% O_2 [%]	7 months stability after 4 weeks	23
Re(I) complex with oxadiazole-derived diamine ligand/ phosphorescence	Polystyrene nanofibers	$I_0/I_{100} = 4.14$	100.0% N_2 to 100.0 O_2 [%]	Good short-term Photostability Long-term stability: Not mentioned	24
Iridium(III) complex and Palladium(II) complex/ phosphorescence and decay time	Nanobeads made up of poly(methylmethacrylate), polystyrene, polyurethanes, ethylcellulose, and other polymers	In ethyl cellulose beads $I_0/I_{air\ sat} = 3.6$	0–300 Torr pO_2	Not mentioned	25
Pyrene	Ionic qtaining elecrospun ethyl cellulose	$I_0/I_{100} = 2.93$	100.0% N_2 to 100.0% O_2 [%]	Short-term stability: 45 min under continuous irradiation Long-term stability: 100 days under ambient conditions	This study

2. Results and discussion

2.1. Choice of matrix

Type of matrix material is of great importance in gas sensor designs and affects the characteristics of the sensor such as sensitivity and stability. The modification of the matrix material can overcome some problems such as photodegradation of the indicator dye and/or leaching of the dye from the matrix. Moreover, the employed matrix affects the gas diffusion rate, resulting in different response times and relative signal changes. Some previous investigations have shown that when compared with the polymeric materials, the green chemistry reagents ionic liquids provided better stability for the sensing agent and higher gas adsorption capacity.[33−39] The solubility of oxygen gas in ionic liquids was reported as 10 to 20 times higher than that in aqueous solutions, conventional solvents, and solid polymer matrices.[40] O_2 is found to be one of the most and reversibly soluble among other gases such as methane, ethane, argon, nitrogen, carbon monoxide, and hydrogen in the ionic liquid of 1-butyl-3-methylimidazolium tetrafluoroborate. In our proposed sensor, the ionic liquids not only increased the gas solubility of the matrix but also behaved as an internal buffering system that increased the stability of the pyrene dye even under the ambient air of the laboratory conditions. Ionic liquids are formed of cationic and anionic parts, some of which acted as Lewis and Brønsted acids or bases. Thus, they behave as self-buffering systems in that they resist ionization as a function of changes in pH.[41,42] Additionally, the presence of ionic liquid in the sensing cocktail facilitated the electrospinning process by increasing the electrical conductivity in the media. The structures of the employed ionic liquids are shown in Figure 1.

2.2. SEM images of the sensing materials

In the present study, we utilized pyrene molecule in the solid matrix of thin films and porous surfaces modified with different ionic liquids. The sensing slides fabricated by the electrospinning technique were characterized with SEM photographs. The cocktails prepared from EC polymer were different from those prepared from polymethyl methacrylate polymer. They resulted in nano- and microporous bulky structures rather than nanofiber forms. The SEM images of electrospun slides of C1–C6 are shown in Figure 2. While the fluoride-based IL-containing slides of C1, C2, C3, and C5 exhibited a significantly higher porous characteristic, the slides of C6, which did not contain any ionic liquid, exhibited a less porous structure. The average pore diameters of C1, C2, C3, and C5 were in the range of 500 nm to 15 μm. The higher porous characteristic containing many empty spaces and holes causes higher gas diffusion within the network. In the case of C2, which contained hydrophobic ionic liquid, IL-II, the pores were larger (microscale) and thus the sensing capability of the sensor slides was enhanced. In the case of C1, C3, and C5, which contained hydrophilic ILs, the structure was still highly porous with smaller pore diameters. In the case of C6, which did not contain any ionic liquid, we did not observe a microscale porous structure. The higher porous structure and the surface area observed for C1–C3 is compatible with our sensitivity results. The conditions of the electrospinning process were optimized in terms of cocktail composition, working distance, viscosity, and dye concentration. The other parameters, such as temperature and humidity, were kept constant; however, they could be tuned in order to increase porosity at the film surface and thus sensitivity could be enhanced.[43]

2.3. Steady state fluorescence measurements

We recorded both steady state and lifetime based data of the immobilized pyrene dye for different concentrations of oxygen. The experiments were performed for ethanolic solution forms, thin films, and electrospun sensing slides prepared from cocktails of C1–C6 (see Table 2). The emission-based data are given in Table 3. The

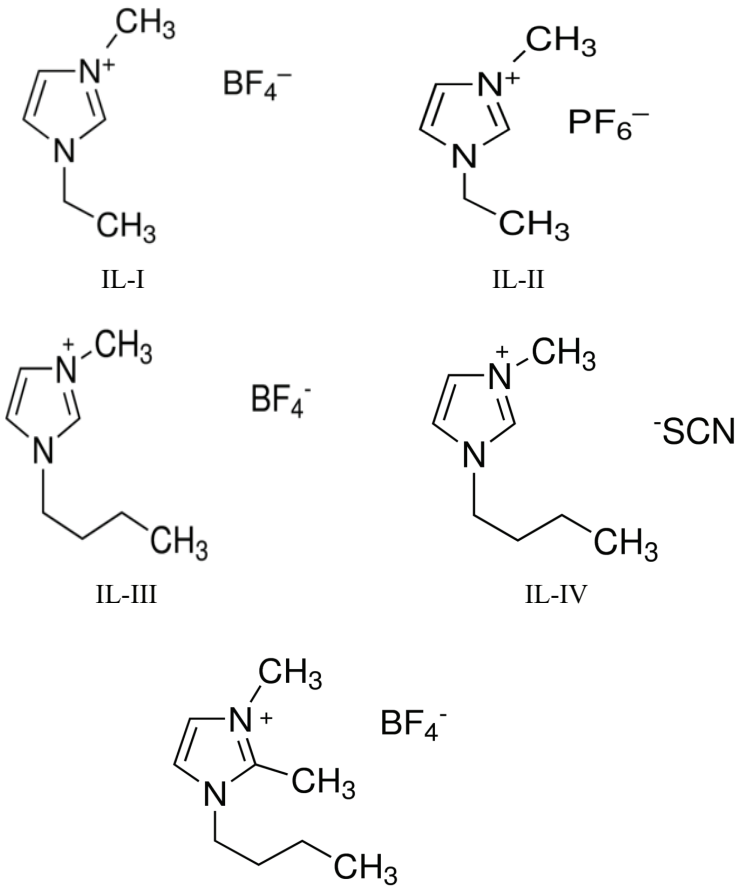

Figure 1. Structure of the employed ionic liquids, IL-I: 1-ethyl-3-methylimidazolium tetrafluoroborate ([EMIM][BF_4]), IL-II: 1-butyl-3-methylimidazolium hexafluorophosphate ([BMIM][PF_6]), IL-III: 1-butyl-3-methylimidazolium tetrafluoroborate ([BMIM][BF_4]), IL-IV: 1-butyl-3-methylimidazolium thiocyanate ([BMIM][SCN]), and IL-V: 1-butyl-2,3-dimethylimidazolium tetrafluoroborate ([BM_2IM][BF_4]).

emission spectra of pyrene in different matrices are also shown in Figure 3. The pyrene dye exhibited strong fluorescence when excited at 340 nm. The dye showed emission maxima at 370 and 388 nm in ethanolic solution. When doped into ethyl cellulose polymer, both in thin film and in electrospun forms, it exhibited a slightly red shift to 374 and 391 nm and a new peak appeared at 470 nm (Figure 3). The fluorescence at 374 and 391 nm originates from the monomers of pyrene molecule, while the peak at 470 nm is expected to originate from the excimer forms. A pyrene molecule in ground state interacts with a pyrene molecule in excited state in order to form an excimer. This formation of excimer is diffusion-controlled and is due to the high diffusion coefficient of pyrene in the ethyl cellulose matrix. It can be concluded that the fluorescence characteristics of the pyrene molecule are significantly affected by the employed polymer matrix, which gained the superior characteristics of a high Stokes shift for sensor studies. The new peak at 470 nm is also useful for the development of more advantageous sensors working at the visible region of the electromagnetic spectrum. It is also known that the oxygen sensitivity of the emission band of the excimer of pyrene at 470 nm is higher than the sensitivity of the monomer emission band.[2,18] This is in accordance with our results with higher relative signal changes (RSC) obtained at 470 nm. It is known that some of the room temperature ionic liquids (RTILs) have intrinsic

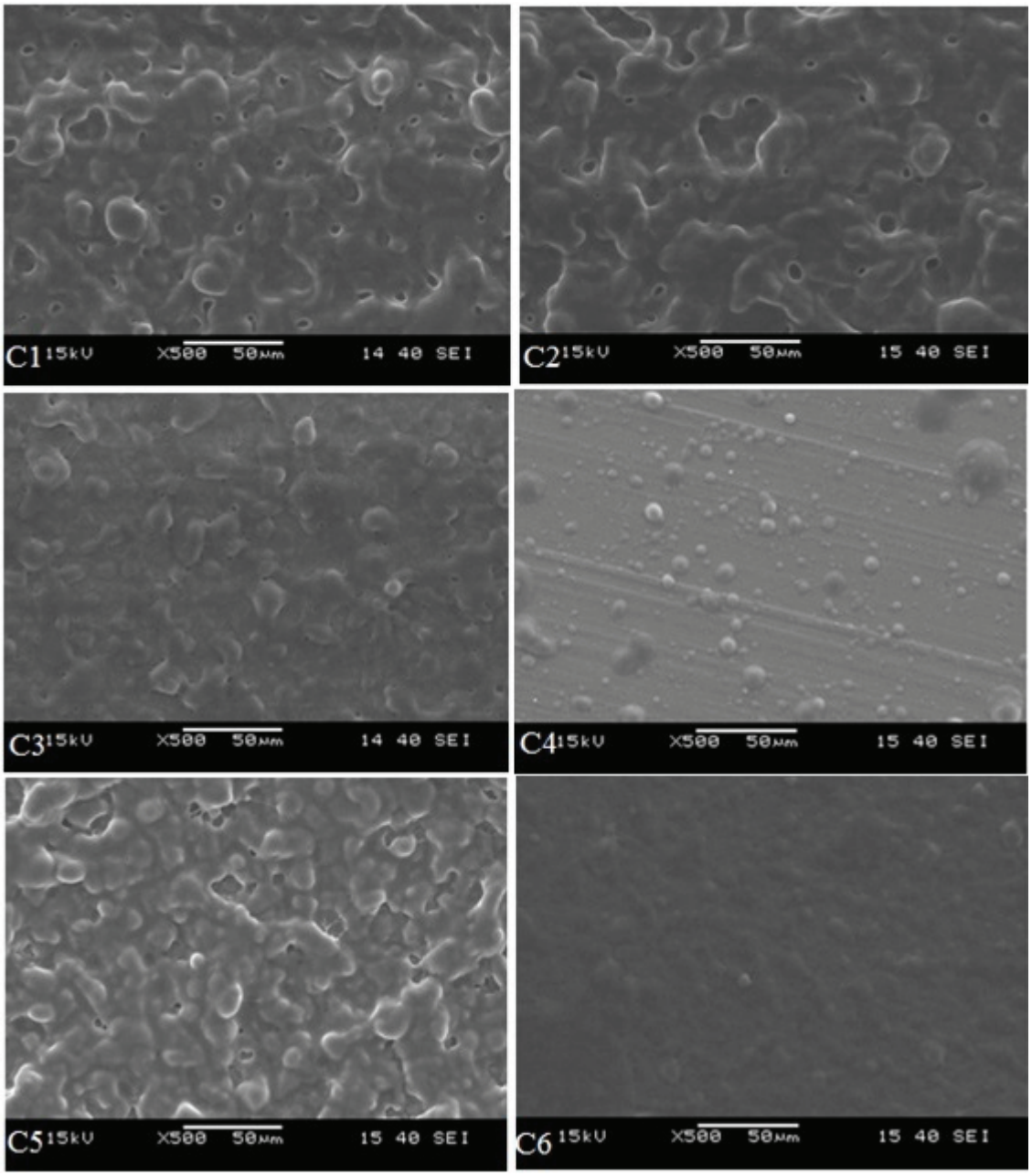

Figure 2. SEM photographs of electrospun sensing slides prepared from C1–C6 (500×).

fluorescence characteristics.[44] Thus, the possible interference of the RTILs on the emission of pyrene dye was also checked. The results showed that the spectral characteristics of the pyrene dye both at 370 and 470 nm were not affected by the ionic liquid.

2.4. Fluorescence lifetime-based measurements

The fluorescence lifetimes of the employed electrospun slides and thin films are shown in Table 3. It is known that the fluorescence decay follows an exponential decay law, which was given by Istratov and Vyvenko.[45] The fluorescence lifetime is defined as the average time that the molecule spends in the excited state prior

Table 2. Compositions of cocktails employed for O_2-sensing with pyrene dye.

Cocktail number	Ionic liquid (48 mg)	Polymer (240 mg)	Dye (10 mg)	Additive (192 mg)
C1	IL-I	EC	Pyrene	DOP
C2	IL-II	EC	Pyrene	DOP
C3	IL-III	EC	Pyrene	DOP
C4	IL-IV	EC	Pyrene	DOP
C5	IL-V	EC	Pyrene	DOP
C6	-	EC	Pyrene	DOP

Table 3. Fluorescence decay times, Stern–Volmer constants and oxygen quenching constants of pyrene dye in fiber and film forms.

PYRENE	$\tau_{0\ (ns),}$ (% dist.)	$\tau_{air\ (ns),}$ (% dist.)	$\tau_{O2\ (100\%)\ (ns),}$ (% dist.)	K_{SV} $[\%]^{-1}$ (lifetime based)	K_{SV} $[\%]^{-1}$ (Intensity based)	kq $([\%]^{-1}ns^{-})$
EtOH	$\tau_1 = 220^a$ (100)	$\tau_1 = 31^a$	-	25^a (atm^{-})	-	1.3×10^{10} L mol^{-1} s^{-1})
C1 Electrospun slide	$\tau_1 = 178$ (100)	$\tau_1 = 156$ (100)	$\tau_1 = 104$ (100)	7.10×10^{-3}	1.47×10^{-2}	3.99×10^{-5}
C1 Film	$\tau_1 = 173$ (100)	$\tau_1 = 146$ (100)	$\tau_1 = 103$ (100)	6.90×10^{-3}	1.45×10^{-2}	3.99×10^{-5}
C2 Electrospun slide	$\tau_1 = 167$ (100)	$\tau_1 = 147$ (100)	$\tau_1 = 102$ (100)	6.40×10^{-3}	1.31×10^{-2}	3.83×10^{-5}
C2 Film	$\tau_1 = 262$ (100)	$\tau_1 = 178$ (100)	$\tau_1 = 89$ (100)	1.96×10^{-2}	1.44×10^{-2}	7.48×10^{-5}
C3 Electrospun slide	$\tau_1 = 156$ (100)	$\tau_1 = 147$ (100)	$\tau_1 = 89$ (100)	7.40×10^{-3}	1.31×10^{-2}	4.74×10^{-5}
C3 Film	$\tau_1 = 153$ (100)	$\tau_1 = 143$ (100)	$\tau_1 = 100$ (100)	5.20×10^{-3}	6.00×10^{-3}	3.40×10^{-5}
C6 Electrospun slide	$\tau_1 = 155$ (100)	$\tau_1 = 129$ (100)	$\tau_1 = 82$ (100)	8.90×10^{-3}	1.07×10^{-2}	5.74×10^{-5}

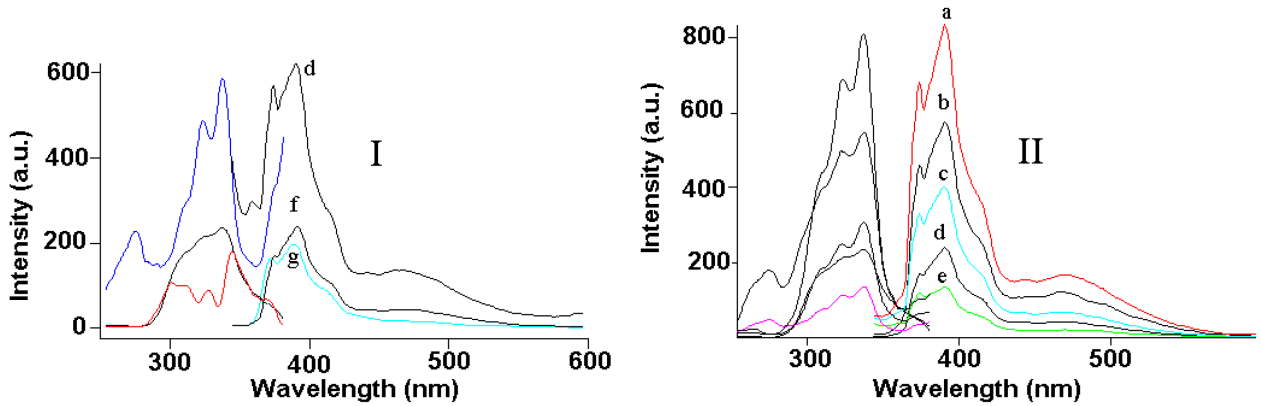

Figure 3. The fluorescence spectra of IL-II containing d) electrospun, f) thin film forms, g) ethanolic solution of pyrene dye, II: The fluorescence spectra of electrospun sensing slides of pyrene dye a) in absence of ionic liquid and in presence of different ionic liquids: b) IL-III, c) IL-V, d) IL-II, and e) IL-IV.

to return to the ground state. Hence, for a single exponential decay, the fluorescence intensity in logarithmic scale due to time gives a straight line and the average time a fluorophore remains in the excited state is equal to the lifetime ($t = \tau$). The average time is not equal to the lifetime in complex multiexponential decays.

The microenvironment of the fluorescent dye also affects the type of decay. Multiexponential decay would be observed in the case of a purity or a heterogeneous matrix.[46] We have found that the decay in the monomeric region of pyrene exhibited similar characteristic in the ethyl cellulose matrix like in the EtOH matrix and is single exponential. This result is in accordance with recently published studies.[18–20,47]

The lifetimes for electrospun slides of C1–C6 ranged from 153 to 262 ns in the absence of oxygen. The immobilization of pyrene in solid ethyl cellulose polymer decreased the lifetime value when compared with the lifetime of pyrene in EtOH. This result is in accordance with Wallace and Thomas, who reported that rate constants of pyrene dye in sodium dodecyl sulfate (SDS) are slower than the rate constants of pyrene in water for oxygen quenching studies.[48] It is also known that the increase in the polar characteristic of the solvent decreases the lifetime value of pyrene. This can also be the reason for the lower lifetime values in all ethyl cellulose matrices except that of C2. The cocktails of C1–C5 had different types of ionic liquids, while C6 did not contain any ionic liquid. In the case of C1 and C3, the lifetime values were not affected considerably by the presence of ionic liquid. In the case of C2, which contained IL-II, the lifetime of pyrene dramatically increased when compared with the IL-free matrix (see Table 3). This result is evidence of decreased rotational movements of the pyrene molecule in the C2 matrix, which contains the only hydrophobic and most viscous ionic liquid (IL-II). It is known that the oxygen sensing capability of a sensor due to quenching depends on both the permeability and diffusion of oxygen gas and the luminescence lifetime in the absence of oxygen, τ_0.[18]

Luminophores with longer τ_0 lifetimes are known to have higher oxygen sensitivities and thus are preferred for oxygen sensor studies. C2, which contained IL-II, exhibited a high τ_0 value of 262 ns, even higher than in solution phase (220 in EtOH), which shows higher oxygen sensitivity and is advantageous for sensor studies. We investigated the effect of oxygen upon the fluorescence lifetime of pyrene solubilized in ionic liquid free and ionic liquid containing ethyl cellulose matrices. The dynamic quenching depends on the viscosity of the solvent and the size of the reactants due to the rate of diffusion controlled mechanism between the reactants.[49] We obtained the highest quenching rate constant value kq = 7.48 $\times$ 10^{-5} $[\%]^{-}$ ns^{-} for C2 from lifetime quenching studies. The lifetime-based and intensity-based Stern–Volmer constants were 1.96 $\times$ 10^{-2} and 1.44 $\times$ 10^{-2}, respectively. The lifetimes obtained are in the range of time scales of diffusion-based bimolecular reactions, which is evidence of dynamic quenching.

2.5. Oxygen sensing studies

The fluorescence intensities of the electrospun slides and thin films at 391 nm and 470 nm were recorded for different oxygen gas concentrations. The fluorescence intensities decreased with the increasing quencher concentrations. The relative signal changes and sensitivities (I_0/I_{100} values) of pyrene dye in different forms are compared in Table 4. The fluorescence quenching of pyrene dye by different concentrations of oxygen in electrospun forms of C2 is also given in Figure 4. The fluorescence of pyrene dye is quenched by triplet oxygen in its excited state via collisions. This type of quenching causes a nonradiative energy transfer and is known as dynamic fluorescence quenching. The amplitude of the dynamic quenching depends on the concentration, temperature, and pressure and the matrix material of the sensing material due to the variations in the frequency of collisions. If the quenching of fluorescence is purely dynamic, both the fluorescence intensity and the fluorescence lifetime are affected by the concentration of O_2. The relation between the oxygen concentration and the fluorescence lifetimes and intensities are defined by the following Stern–Volmer equation:[46]

$$I_0/I = \tau_0/\tau = 1 + K_{SV}[O_2] = 1 + kq\tau_0[O_2], \quad (1)$$

where I_0 and I are the fluorescence intensities and τ_0 and τ are the fluorescence lifetimes in the absence and presence of oxygen, respectively. K_{SV} is the Stern–Volmer constant and kq is the quenching constant, which is related to the diffusion ability of oxygen through the matrix. When the ratio of I_0/I or τ_0/τ versus $[O_2]$ was plotted, a straight line with an intercept at 1 was obtained for ideal and homogeneous environments. The K_{SV} value, which is the measure of sensor sensitivity, can be obtained from the slope of the line. If there are heterogeneous sites containing the luminophore in the solid matrix, then the Stern–Volmer plot is not linear. Most optical oxygen sensors have such unfavorable nonlinear Stern–Volmer plots.[46,50]

Table 4. Comparison of relative signal changes and sensitivities (I_0/I_{100} values) of pyrene dye in electrospun and in thin film forms.

Sensing slide	I_0/I_{100} (390 nm)	I_0/I_{100} (470 nm)	Intensity based Stern–Volmer equation	R^2	Relative signal change (%)	
					390 nm	470 nm
C1 Electrospun slide	2.61	-	y = 0.0147x + 1	R^2 = 0.9765	62	-
C2 Electrospun slide	2.34	2.80	y = 0.0131x + 1	R^2 = 0.9981	57	64
C2 film	2.40	2.93	y = 0.0144x + 1	R^2 = 0.9995	58	66
C3 Electrospun slide	2.40	2.66	y = 0.0131x + 1	R^2 = 0.9964	58	62
C3 film	1.64	1.71	y = 0.0060x + 1	R^2 = 0.9945	39	41
C4 Electrospun slide	1.98	2.88	y = 0.0133x + 1	R^2 = 1.0000	49	65
C5 Electrospun slide	1.92	2.40	y = 0.0093x + 1	R^2 = 0.9974	48	58
C6 Electrospun slide	2.07	2.89	y = 0.0107x + 1	R^2 = 0.9997	52	65

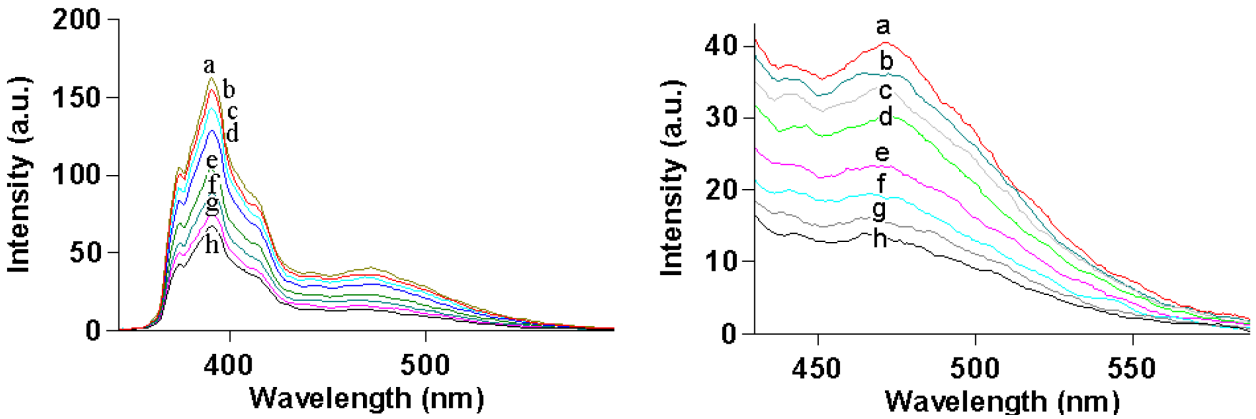

Figure 4. Emission spectra of electrospun sensing slides of C2 after exposure to certain concentrations of O_2: a) 0.0%, b) 5.0%, c) 10.0%, d) 20.0%, e) 40.0%, f) 60.0%, g) 80.0%, h) 100.0% O_2, Inset: Emission spectrum of thin films obtained from C2 in the range of 430–550 nm.

In this study, both IL-free and IL-doped matrices exhibited linear Stern–Volmer plots with regression coefficients mostly more than $R^2 > 0.99$ in a wide oxygen concentration range between 0.0% and 100.0%. We calculated the Stern–Volmer constants and quenching constants based on the fluorescence intensity and fluorescence lifetimes for all matrices (Table 4). The Stern–Volmer constant of the ionic liquid containing sensing slides was enhanced in the range of 6–14 times with respect to the ionic liquid free ones. This is not a surprising result for us as we had expected an enhancement in the diffusion of oxygen gas through the ionic liquid modified matrices as ionic liquids are known for their high gas solubilities, especially for CO_2 and O_2 gases. The ratio I_0/I_{100} is also representative of the sensitivity of a sensor, where a higher value means higher

sensitivity. We give both the I_0/I_{100} values of the monomer and excimer emissions of pyrene at 390 and 470 nm, respectively, in Table 4. As we see from this table, the oxygen sensitivity of the emission band of the excimer of pyrene at 470 nm is higher than the sensitivity of the monomer emission band as we obtained higher relative signal changes at 470 nm.

2.6. Effect of type of ionic liquid on sensing properties

We used five different imidazolium-based ionic liquids in cocktail compounds. The anionic parts of ionic liquids were BF_4^-, PF_6^-, and CN^-. The cocktails C1–C5 contain different types of ionic liquids, while C6 is IL-free. After exposure to O_2, relative signal changes extending from 48% (C5 electrospun) to 62% (C1 electrospun) were obtained for monomer quenching at 390 nm (see Table 4). We obtained the best K_{SV} values for the cocktails of C1–C3, which contained ionic liquids with anionic fluoride groups. This result shows that the anionic groups containing fluoride such as BF_4^- or PF_6^- increase the solubility of oxygen in the sensor matrix. The enhancement of oxygen solubility in the presence of fluorine is also mentioned in the literature.[23,51,52] In the case of ionic liquid-free sensing slides I_{390} nm/I_{470} nm was 4.0, while for the ionic liquid-containing ones this value increased up to 6.0 under nitrogen atmosphere. Under oxygen atmosphere the I_{390} nm/I_{470} nm value enhanced more dramatically from 2.98 up to 6.85, which indicates that in the presence of oxygen the excimer emission dramatically decreases for ionic liquid-containing sensing slides. This resulted in a higher sensitivity to oxygen at 470 nm. The oxygen sensitivity extended to 65% for all cocktail types at 470 nm with respect to 390 nm. However, the fluorescence intensity at 470 nm attributed to excimer emission was smaller than that of monomer emission. Moreover, the sensitivity to oxygen (I_0/I_{100} value) at 470 nm was not significantly affected by the presence of ionic liquid or ionic liquid type.

2.7. Sensing properties of electrospun slides and thin films

Figure 5 shows a comparison of gathered Stern–Volmer plots of the C2 and C3 in electrospun and thin film forms after exposure to various concentration of O_2 from 0.0% to 100.0%. It is observed that all Stern–Volmer plots exhibited good linear relationships with increasing oxygen concentrations. The calculated Stern–Volmer constants (K_{SV}) are shown in Table 3. According to the data, the K_{sv} values of electrospun and thin film forms of C1 and C2 are very close to each other, while the K_{sv} value of the electrospun slides obtained from C3 is approximately 2.2-fold higher than the K_{sv} value of C3 thin film.

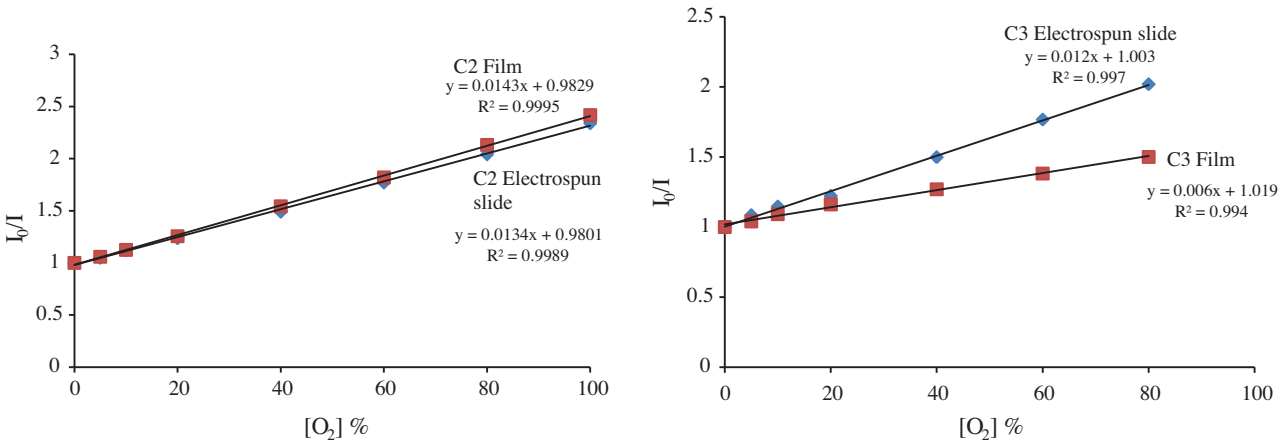

Figure 5. Comparison of gathered Stern–Volmer plots of the electrospun sensing slides and thin films of C2 and C3.

2.8. Response to dissolved oxygen

Mixtures of N_2 and O_2 gases with different compositions in the range of 0.0–100.0% (v/v) O_2 were prepared to obtain oxygenated-water solutions. The sensing films and electrospun slides prepared from C1, C3, C4, and C5 had the problem of leaching in aqueous media and were only employed for gas sensing purposes. It is known that leaching is a significant problem in optical sensor designs and most of the oxygen sensors work for gaseous oxygen measurements. However, the use of hydrophobic IL-II in the sensor composition not only enhanced the sensor response for gaseous oxygen but also gave us the opportunity to use our sensing slides for dissolved oxygen measurements in aqueous media without any leaching problem. Leaching was checked many times by measuring the probable fluorescence signal changes after leaving the slides for at least 30 min in water before the experiments. Figure 6 shows the response of sensor films prepared from C2 towards various concentrations of dissolved oxygen in water. The I_0/I_{100} value of the thin film form of C2 was 2.22, where I_0 and I_{100} represent the fluorescence intensity for 100.0% N_2 and O_2 saturated water, respectively. The dissolved oxygen concentration is taken as 0.273 mmol L^{-1} at 25 °C under 21.0% oxygen atmosphere. The resulting oxygen concentrations were calculated by using Henry's law. The Stern–Volmer plot for dissolved O_2 measurements is shown in the inset of Figure 6. The linear relationship can be described by the Stern–Volmer equation y = 0.8054x + 1.1878. The slope of the graph represents the Stern–Volmer constant, K_{sv} = 0.8054 L $mmol^{-1}$. The regression coefficient was R^2 = 0.9972 with linearity up to the dissolved oxygen concentration of 1.3 mmol L^{-1}. The limit of quantification was the lowest measured concentration of dissolved oxygen with accuracy and was found as 0.065 mmol L^{-1} from the calibration plot. The sensor exhibited good linearity over a wide concentration range, which facilitates the calibration of the oxygen sensor in practical applications. Furthermore, both the Stern–Volmer constant and I_0/I_{100} value (2.33) showing the sensitivity of the sensor are higher than those of many of the dissolved oxygen sensors described in the literature. Xiong et al. designed a dissolved oxygen sensor containing ruthenium complex immobilized on silica–Ni–P composite coating and found a K_{sv} value of 0.0761 L $mmol^{-1}$. In another study they found the sensitivities of different fluorinated xerogels immobilized with ruthenium(II) complex in the range of 1.32–3.31.[52,53] Xuea et al. found Stern–Volmer constants (K_{sv}) of 0.04, 0.08, and 0.41 $(mg/L)^{-1}$ for different kinds of sensors.[54]

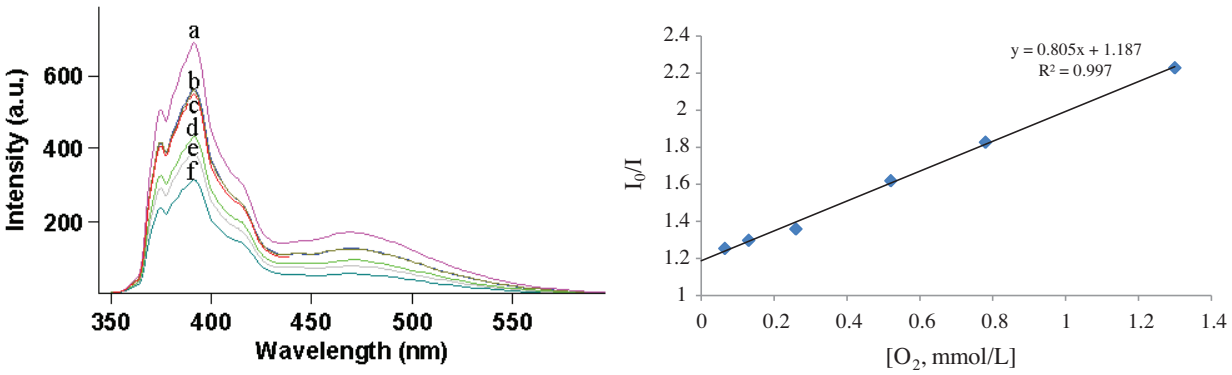

Figure 6. Dissolved oxygen response of electrospun nanofibers obtained from C2 a) 0.0%, b) 5.0%, 10.0%, c) 20.0%, d) 40.0%, e) 60 % f) 100.0% O_2 concentrations, Inset: Stern–Volmer plot for dissolved oxygen measurements.

2.9. Response and regeneration times

Response and regeneration times were measured for electrospun and thin film forms of C2 and C3. Figure 7 illustrates the kinetic response of electrospun slides prepared from C2 after exposure to different O_2 con-

centrations. Response time is defined as the time passed to reach 90.0% of its original signal intensity (τ_{90}) when the gas is changed. The response time of electrospun slides prepared from C2 was in the range of 6–20 s. Regeneration time was 7 s depending on the oxygen concentration. After six replicate measurements with 100.0% N_2 and O_2 gases, the standard deviation of upper and lower signal levels was found to be 600.2 ± 8.2 and 242.3 ± 0.8 (n = 7), respectively.

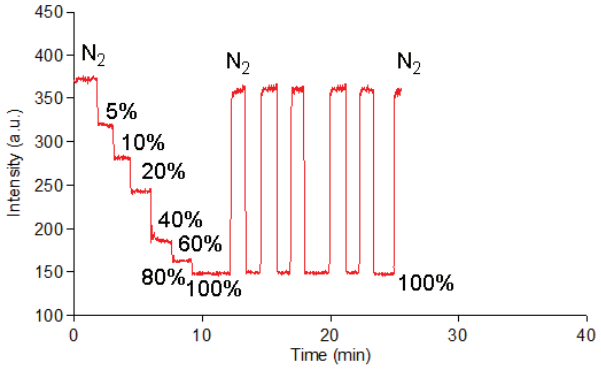

Figure 7. Emission based kinetic response of electrospun sensing slides prepared from C2 after exposure to N_2 (g) and certain concentrations of 0.0%, 5.0%, 10.0%, 20.0%, 40.0%, 60.0%, 80.0%, 100.0% O_2 (g).

The response time of electrospun C3 slides was in the range of 7–28 s, depending on the oxygen concentration. After seven replicate measurements with 100.0% N_2 and O_2 gases, the standard deviation of upper and lower signal levels was found to be 362.5 ± 1.6 and 150.2 ± 0.4, respectively.

The response time for C2 film was longer and was found to be in the range of 9 and 26 s. The regeneration time of C2 film was 23 s. The response time for C3 was in the range of 5–16 s. The regeneration time of C3 film was 16 s. The response times for oxygen sensing of electrospun slides prepared from C2 and C3 were shorter when compared with their thin film forms. All of the films and slides could be totally regenerated in less than 8 s after exposure to 100.0% and 0.0% O_2 (g) for 7 replicate measurements.

Kinetic response studies showed that the ionic liquid-doped electrospun slides and films could be easily regenerated many times. They exhibited stable and reproducible oxygen sensing properties.

The applicability of the sensing system for real samples was tested with the ambient air atmosphere of the laboratory (21.0% O_2 (g)). The resulting concentrations of the oxygen gas measured with the sensing film and fiber prepared from C2 was 21.7 ± 0.4% and 20.9 ± 0.4% O_2 (g), respectively. These results reveal the capability of the proposed sensing design for the determination of oxygen gas in real samples without considerable error. The selectivity of the sensor was also checked with CO_2 gas, which is one of the most abundant gases after O_2 in the air atmosphere, and no cross-sensitivity was observed.

2.10. Short-term sensor stability

Pyrene dye has many advantages as a luminophore for the design of oxygen sensors because of its high quantum yield value, good sensitivity for pressure, and low coefficient of temperature.[6,7] However, photodegradation of PAHs in solutions is a well-known problem; it is an oxidative process accelerated by the presence of photo-initiators.[7] The photodegradation process is also affected by temperature, light intensity, and amount of dissolved oxygen.[8] This is an important problem for the application of pyrene in optical sensing designs. Thus, we checked the short-term stability of the sensing slides prepared from C2 by exposure of continuous radiation

at 390 nm and 470 nm under air atmosphere (21.0% O_2) (Figure 8). The pyrene dye did not exhibit any photodegradation during the experiment time (for 45 min) after continuous irradiation. This result indicates that pyrene dye immobilized in solid ethyl cellulose matrix (C2 composition) was stable against irradiation. The mechanism of pyrene degradation under UV radiation was proposed in the literature as both an energy transfer from the pyrene to the singlet oxygen and an electron transfer from the excited singlet state of pyrene to molecular oxygen.[55,56] Clark et al. have reported that the photolysis of pyrene is substantially faster in the presence of oxygen and also requires water.[57] The immobilization of pyrene in a polymer matrix both in the presence and in the absence of ionic liquid supplied a hyrophobic matrix for the dye and enhanced the short-term photostability under continuous irradiation.

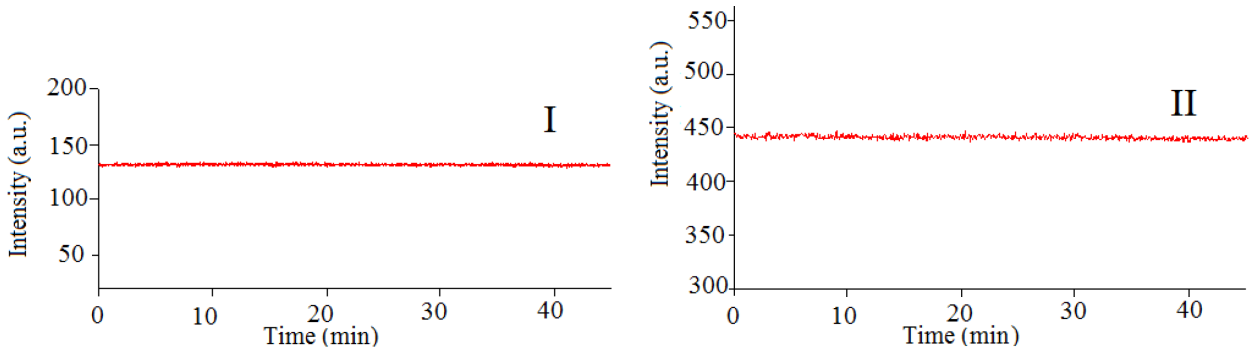

Figure 8. Stability of sensing slides prepared from C2 under continuous irradiation at I) 470 nm and II) 390 nm.

2.11. Long-term sensor stability

Figure 9 illustrates the stability of the sensing films prepared from C2, which were stored at room temperature in a closed box in laboratory conditions. The equations of the calibration plots obtained from C2 were $y = 0.0131x + 1$ and $y = 0.0141x + 1$, at the beginning and after 100 days, respectively. No significant change in the fluorescence lifetimes, intensities, or slopes of the calibration plots of the electrospun slides was observed after 100 days for the IL-II containing cocktails. The composition of C3 had lost its original fluorescence intensity by 29.0% but still had efficient luminescence for O_2 measurements. The slope of the calibration plots obtained from C3 also did not exhibit a significant change after 100 days. This was a gratifying result as the pyrene molecule is well known for its low photostability characteristics. The storage lifetime measured in this work is the longest reported lifetime for pyrene-based sensors. This can be attributed to the presence of hydrophobic IL-II, which protects the sensor from acid–base and/or oxidative–reductive attacks.

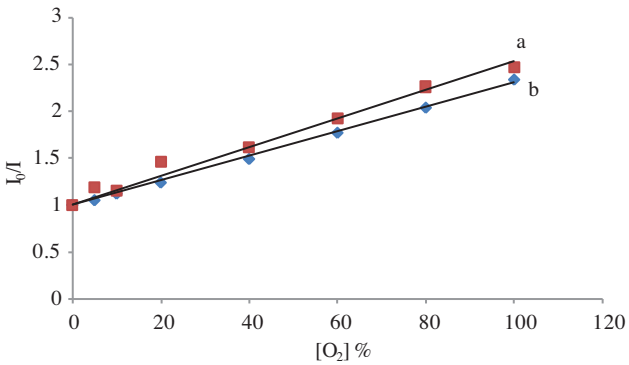

Figure 9. The calibration plots of the sensing slides prepared from C2 stored in ambient laboratory conditions in a closed box: a) at the beginning, b) after 100 days.

The fluorescence characteristics of the pyrene were improved, such as a new emission band at 470 nm and high Stokes shift for sensor studies, when doped in ionic liquid modified ethyl cellulose matrix. The use of the ionic liquids significantly increased the sensitivity and the stability of the pyrene dye in ethyl cellulose-based thin films and electrospun slides. The oxygen sensitivity of the emission band at 470 nm was higher than the sensitivity values obtained for 390 nm. The ionic liquid 1-butyl-3-methylimidazolium hexafluorophosphate ($[BMIM^+][PF_6^-]$) was used as an additive in the sensor matrix for the first time for dissolved oxygen measurements. The hydrophobic character of the ionic liquid enabled the sensor to retain the storage stability of the ethyl cellulose matrix and prevented leaching in aqueous media.

Basu et al. have reported that the degradation of pyrene was due to the loss of dye in the coatings by evaporation assisted by diffusion.[58] This evaporation will be slower in a solid polymer matrix when compared with the solution phase. The presence of ionic liquid in the ethyl cellulose matrix additionally enhanced the long-term stability of the dye. Room temperature ionic liquid was expected to fill the free volumes of the porous polymer film and prevent the diffusion and the evaporation of the dye from the film surface. Moreover, for both gaseous and dissolved oxygen sensing studies, the buffer characteristic of ionic liquid acted as a sink for the attacks of oxidative/reductive and acid/base compounds, leading to an enhancement in the long-term stability of the pyrene dye in the sensor matrix. The short-term photostability of the dye was also enhanced in the ionic liquid-modified solid matrix and no photobleaching was observed after continuous irradiation for 45 min. The sensors presented here exhibited a fast, linear, and reversible response to oxygen in a wide concentration range of 0.0%–100.0% O_2 (g). The limit of quantification of the dissolved oxygen sensor was 0.065 mmol L^{-1}. The I_0/I_{100} value of the sensing slides was 2.93 and 2.33 for gaseous and dissolved oxygen measurements, respectively. This sensitivity we obtained with pyrene dye is higher than what we obtained for $Ru(bipy)_3^{2+}$ in our previous studies. The method can be applied for both dissolved and gaseous oxygen measurements. The presence of ionic liquids also facilitated the electrospinning process, providing electrical conductivity within the matrix. The electrospun slides offered larger and porous surfaces with respect to continuous thin films, which resulted in increased sensitivity.

3. Experimental

3.1. Materials

The pyrene dye was supplied by Sigma Aldrich. The ethyl cellulose polymer (EC, ethoxy content of 48%) and dioctyl phthalate (DOP) were from Aldrich. The hydrophobic ionic liquid IL-II: 1-butyl-3-methylimidazolium hexafluorophosphate ($[BMIM^+][PF_6^-]$), and the hydrophilic ionic liquids IL-I: 1-ethyl-3-methylimidazolium tetrafluoroborate ($[EMIM^+][BF_4^-]$), IL-III: 1-butyl-3-methylimidazolium tetrafluoroborate ($[BMIM^+][BF_4^-]$), IL-IV: 1-butyl-3-methylimidazolium thiocyanate ($[BMIM^+][SCN^-]$), and IL-V: 1-butyl-2,3-dimethylimidazolium tetrafluoroborate ($[BM_2IM^+][BF_4^-]$) were supplied by Fluka and Merck (Figure 1). Oxygen and nitrogen gases were of 99.9% purity and obtained from the Erma Company, İzmir, Turkey.

3.2. Instrumentation

3.2.1. Steady state and time resolved fluorescence measurements

A Varian Cary Eclipse spectrofluorometer with the light source of a xenon flash lamp was used for steady state fluorescence measurements.

The Time Correlated Single Photon Counting (TCSPC) system from Edinburgh Instruments (UK) of

FLS920 was used for fluorescence lifetime measurements. The excitation was performed with a 367.8 nm pulsed laser source with a pulse width of 790.4 ps. The emission data were collected at 390 nm. The lifetime data were collected by using reconvolution with a weighted, nonlinear least-squares method. In all of the experiments, the chi-square values (χ^2) were less than 1.2 and the residuals trace symmetrically distributed around the zero axes.

3.2.2. Electrospinning device

A programmable syringe pump (Top Syringe Pump Top-5300) and a high voltage power supply (Gamma High Voltage ES30) were used for electrospinning. The surface morphology of the electrospun slides was studied using a scanning electron microscope (SEM) (6060-JEOL JSM).

3.2.3. Gas sensing studies

The O_2 and N_2 gases were mixed in a Sonimix 7000A gas blending system in order to obtain different oxygen concentrations in the range of 0.0%–100.0%. The output flow rate of the gas mixture was fixed at 498 mL min^{-1}. Gas mixtures were employed on the sensing slides via a diffuser needle under ambient conditions for 1 min and then the spectral data were recorded. For the dissolved oxygen sensing measurements, the nitrogen and oxygen gases at different concentrations (0.0%, 0.5%, 1.0%, 2.0%, 5.0%, 10.0%, 20.0%, 40.0%, 60.0%, and 100.0% O_2) were flowed into ultrapure water for 10 min. The spectra were recorded after closing the gas flow in order to prevent bubbles in the cuvette.

3.2.4. Preparation of electrospun sensing slides

Several sensing slides were prepared from different cocktail compositions. The compositions of the cocktails are shown in Table 2. Briefly, the cocktails C1–C5 were prepared to contain IL-I–IL-V, respectively, while C6 did not contain any ionic liquid. The homogeneous cocktail solutions were later placed in a 10-mL plastic syringe for the electrospinning process. The syringe had a metallic needle of 0.4 mm inner diameter. The electrode of the high voltage power supply was clamped to the needle tip. The applied voltage was 25 kV, the feed rate of the cocktail solution was 2.0 mL/h, and the tip-to-collector distance was 10 cm. The full device was in a dust-free closed glass cabin at 20.0 °C. After starting the high voltage, the electrical forces acted in opposition to overcome the surface tension of the fluid. Approximately 10 min later, a stream of polymer jet began. The solvent was evaporated and the polymer was coated on the clean aluminum foil, forming a porous structure.

3.2.5. Preparation of thin films

The thin films were also prepared with the same compositions of cocktails that were used for the construction of electrospun slides. The homogeneous cocktails were spread onto a 125-μm Mylar type polyester support by the knife coating technique. Immediately after the coating process, the films were taken into a THF saturated desiccator for drying. Thicknesses of the films were found to be 5.43 $\pm$ 0.13 μm (n = 8) (Tencor Alpha Step 500 Prophylometer). Each sensing film was prepared to be 1.2 cm in diameter and was fixed diagonally in the cuvette for the spectral measurement.

Acknowledgments

Funding for this research was provided by the Scientific Research Funds of Dokuz Eylül University: 2012.KB.FEN.049 and 2009.KB.FEN.075. We also thank the Center for Fabrication and Application of Electronic Materials (EMUM) in İzmir, Turkey, and TÜBİTAK–Kariyer Project–104M268.

References

1. Wang, X. D.; Wolfbeis, O. S. *Anal. Chem.* **2013**, *85*, 487–508.
2. Basu, B. J.; Thirumurugan, A.; Dinesh, A. R.; Anandan, C.; Rajam, K. S. *Sensor. Actuat. B-Chem.* **2005**, *104*, 15–22.
3. Gouterman, M. J. *Chem. Educ.* **1997**, *74*, 697–702.
4. Fujiwara, Y.; Amao, Y. *Sensor. Actuat. B-Chem.* **2003**, *89*, 187–191.
5. Fujiwara, Y.; Amao, Y. *Sensor. Actuat. B-Chem.* **2003**, *89*, 58–61.
6. Ishiji, T.; Kaneko, M. *Analyst* **1995**, *120*, 1633–1638.
7. Fujiwara, Y.; Amao, Y. *Sensor. Actuat. B-Chem.* **2002**, *85*, 175–178.
8. Sharma, A.; Wolfbeis, O. S. *Spectroscopy* **1988**, *42*, 1009–1011.
9. Lee, E. D.; Werner, T. C.; Seitz, R. *Anal. Chem.* **1987**, *59*, 279–283.
10. Xu, W.; Schmidt, R.; Whaley, M.; Demas, J. N.; Degraff, B. A.; Karikari, E. K.; Farmer, B. L. *Anal. Chem.* **1995**, *67*, 3172–3180.
11. Lubbers, D. W.; Opitz, N. *Sensor. Actuat. B-Chem.* **1983**, *4*, 641–654.
12. Oter, O.; Ribou, A. C. *J. Fluoresc.* **2009**, *19*, 389–397.
13. Ribou, A. C.; Vigoa, J.; Kohenb, E.; Salmon, J. M. *J. Photoch. Photobio. B* **2003**, *70*, 107–115.
14. Clark, C. D.; De Bruyn, W. J.; Ting, J.; Scholle, W. *J. Photoch. Photobio. A* **2007**, *186*, 342–348.
15. Kubát, P.; Civiš, S.; Muck, A.; Barek, J.; Zima, J. *J. Photoch. Photobio. A* **2000**, *132*, 33–36.
16. Fujiwara, Y.; Amao, Y. *Talanta* **2004**, *62*, 655–660.
17. Bekiari, V.; Lianos, P. *J. Colloid Interf. Sci.* **1996**, *182*, 304–305.
18. Basu, B. J.; Rajam, K. S. *Sensor. Actuat. B-Chem.* **2004**, *99*, 459–467.
19. Hrdlovi, P.; Kollár, J.; Chmela, Š. *J. Photoch. Photobio. A* **2004**, *163*, 289–296.
20. Serban, B.; Costea, S.; Buiu, O.; Cobianu, C.; Diaconu, C. In *CAS 2012*, Proceedings of the International Semiconductor Conference, Sinaia, Romania, 15–17 October 2012; IEEE Romania Section Electron Device Chapter: Romania, 2012, pp. 265–268.
21. Zhang, H.; Lei, B.; Mai, W.; Liua, Y. *Sensor. Actuat. B-Chem.* **2011**, *160*, 677–683.
22. Wu, X.; Song, L.; Li, B.; Liu, Y. *J. Lumin.* **2010**, *130*, 374–379.
23. Estella, J.; Wencel, D.; Mooreb, J. P.; Sourdaine, M.; McDonagh, C. *Anal. Chim. Acta* **2010**, *666*, 83–90.
24. Wang, X. F. *J. Lumin.* **2013**, *134*, 508–514.
25. Borisov, S. M.; Mayr, T.; Mistlberger, G.; Waich, K.; Koren, K.; Chojnacki, P.; Klimant, I.; Talanta **2009**, *79*, 1322–1330.
26. Fuller, J.; Carlin, R. T.; De Long, H. C.; Haworth, D. *Chem. Commun.* **1994**, *3*, 299–300.
27. Rogers, R. D.; Seddon, K. R. In *Ionic Liquids III: Fundamentals, Challenges, and Oppurtunities, ACS Symposium Series*; American Chemical Society: Washington, DC, USA, 2005.
28. Rogers, R. D.; Seddon, K. R. In *Ionic Liquids: Industrial Applications for Green Chemistry, ACS Symposium Series 818*; American Chemical Society: Washington, DC, USA, 2002.
29. Baker, G. A.; Baker, S.; Pandey, S.; Bright, F. V. *Analyst* **2005**, *130*, 800–808.
30. Berthod, A.; He, L. F.; Armstrong, D. W. *Chromatographia* **2001**, *53*, 63–68.
31. Poole, C. F. *J. Chromatogr. A* **2004**, *1037*, 49–82.
32. Armstrong, D. W.; He, L. F.; Liu, Y. S. *Anal. Chem.* **1999**, *71*, 3873–3876.
33. Ongun, M. Z.; Oter, O.; Sabancı, G.; Ertekin, K.; Celik, E. *Sensor. Actuat. B-Chem.* **2013**, *183*, 11–19.

34. Aydogdu, S.; Ertekin, K.; Suslu, A.; Ozdemir, M.; Celik, E.; Cocen, U. *J. Fluoresc.* **2011**, *21*, 607–613.
35. Oter, O.; Ertekin, K.; Topkaya, D.; Alp, S. *Sensor. Actuat. B-Chem.* **2006**, *117*, 295–301
36. Oter, O.; Ertekin, K.; Topkaya, D.; Alp, S. *Anal. Bioanal. Chem.* **2006**, *386*, 1225–1234.
37. Oter, O.; Ertekin, K.; Derinkuyu, S. *Talanta* **2008**, *76*, 557–563.
38. Borisov, S. M.; Waldhier, M. C.; Klimant, I.; Wolfbeis, O. S. *Chem. Mater.* **2007**, *19*, 6187–6194.
39. Bates, E. D.; Mayton, R. D.; Ntai, I.; Davis, J. H. *J. Am. Chem. Soc.* **2002**, *124*, 926–927.
40. Anthony, J. L.; Maginn, E. J.; Brennecke, J. F. *J. Phys. Chem. B* **2002**, *106*, 7315–7320.
41. MacFarlane, D. R.; Pringle, J. M.; Johansson, K. M.; Forsyth S. A.; Forsyth M. *Chem. Commun.* **2006**, *106*, 1905–1917.
42. Cole, A. C.; Jensen, J. L.; Ntai, I.; Tran, K. L. T.; Weaver, K. J.; Forbes, D. C.; Davis, J. H. J. *J. Am. Chem. Soc.* **2002**, *124*, 5962–5963.
43. Deitzel, J. M.; Kleinmeyer, J.; Tan, N. C. *Polymer* **2001**, *42*, 261–272.
44. Delgado, J. M.; Raymundo, A.; Vilarigues, M.; Branco, L. C.; Laia, C. A. T. *Chem. Eur. J.* **2014**, *20*, 1–8.
45. Istratov, A. A.; Vyvenko, O. F. *Rev. Sci. Ins.* **1999**, *70*, 1233–1257.
46. Lakowicz, J. R. *Principles of Fluorescence Spectroscopy*; Springer: Germany, 2006.
47. Hrdlovic, P.; Lukac, I. *J. Photoch. Photobio. A* **2000**, *133*, 73–82.
48. Wallace, S. C.; Thomas, J. K. *Radiat. Res.* **1973**, *54*, 49–62.
49. Geiger, M. W.; Turro, N. J. *Photochem. Photobiol.* **1975**, *22*, 273–276.
50. Borisov, S. M.; Vasylevska, A. S.; Krause, C.; Wolfbeis, O. S. *Adv. Funct. Mater.* **2006**, *16*, 1536–1542.
51. Dias, A. M. A.; Freire, M. G.; Coutinho, J. A. P.; Marrucho, I. M. *Fluid Phase Equilibr.* **2004**, *222*, 325–330.
52. Xiong, Y., Xu, J.; Zhu, D.; Duan, C.; Guan, Y. *J. Sol-Gel Sci. Techn.* **2010**, *53*, 441–447.
53. Xiong, X.; Xiao, D.; Choi, M. M. F. *Sensor. Actuat. B-Chem.* **2006**, *117*, 172–176.
54. Xuea, R.; Beherab, P.; Xua, J.; Viapianob, M. S.; Lannuttia, J. J. *Sensor. Actuat. B-Chem.* **2014**, *192*, 697–707.
55. Sigman, M. E.; Schuler, P. F.; Ghosh, M. M.; Dabestani, R. T. *Environ. Sci. Technol.* **1998**, *32*, 3980–3985.
56. Mill, T.; Mabey, W. R.; Lan, B. Y.; Baraze, A. *Chemosphere* **1981**, *10*, 1281–1290.
57. Clark, C. D.; Warren, J. B.; Jackie, T.; William, S. *J. Photoch. Photobio. A* **2007**, *186*, 342–348.
58. Basu, B. J.; Anandan, C.; Rajam, K. S. *Sensor. Actuat. B-Chem.* **2003**, *94*, 257–266.